Positron thermalization and non-thermal trapping in metals

1990 J. Phys.: Condens. Matter 2 9757

(http://iopscience.iop.org/0953-8984/2/49/004)

J. Phys.: Condens. Matter **2** (1990) 9757–9775. Printed in the UK

Positron thermalization and non-thermal trapping in metals

Kjeld O Jensen and Alison B Walker
School of Physics, University of East Anglia, Norwich NR4 7TJ, UK

Received 4 May 1990

Abstract. We have made a detailed study of the thermalization of positrons implanted into metals, using aluminium as an example. This is done by solving the Boltzmann equation for the positron momentum distribution in a homogeneous medium, allowing the positrons to scatter off electrons and phonons. We obtain both the time-dependent and steady-state solutions. The former gives the time evolution of the positron momentum distribution and the average energy and energy loss rate as functions of time after implantation. The full statistical description of the slowing-down process and the inclusion of both electron and phonon scattering mean that our energy loss rates are more accurate than earlier results, which are considerably lower than ours. The steady-state solution gives the momentum distribution from which positrons annihilate. Our formulation allows us to evaluate the influence of non-thermal trapping into defects, such as vacancies, on measurable parameters in positron experiments. The results show that, even if resonances are present in the momentum-dependent trapping rates, the differences between the results from the full calculation and for trapping from a thermal momentum distribution are exceedingly small. Thus we conclude that non-thermal trapping is not important for positron studies of vacancies in metals.

1. Introduction

Positron annihilation is a well established non-destructive technique for studying defects [1–3]. The advent of slow positron beams has, furthermore, in the last decade enabled defect profiling near surfaces and studies of surface phenomena [4]. In a typical experiment, positrons are injected into the material under study either directly from a radioactive source (implantation energies peaking at ~200 keV) or as a monoenergetic beam (energies from a few eV to ~50 keV). Once injected, the positrons scatter elastically and inelastically off ion cores and conduction electrons, and within a picosecond reach energies of about 1 eV followed by a slower approach towards thermal equilibrium. On thermalization, the positrons diffuse until they (in bulk studies) either annihilate or are trapped at open volume defects, where they subsequently annihilate. In surface studies the surface acts as an additional sink for the positrons. Positron defect studies utilize the fact that the annihilation characteristics such as the lifetime and γ-ray energy spectrum are different for positrons annihilating from the bulk compared to the strongly localized states formed in defects. It is an open question whether trapping prior to thermalization is important for the analysis of positron defect measurements and the extraction of defect parameters, e.g. vacancy formation energies. Our main aim of this paper is to answer this question by a detailed study of the thermalization process, using both

0953-8984/90/499757 + 19 $03.50

time-dependent and steady-state solutions of the Boltzmann equation for the positron momentum distribution. In addition to the data on non-thermal trapping, we also provide more general results for the positron slowing down and thermalization, such as energy loss rates.

The influence of non-thermal trapping on the analysis of lifetime spectra has already been discussed by several authors [5–12] in relation to positron measurements on thermally generated defects. All these papers conclude that a sizeable fraction of positrons are trapped prior to thermalization and that this has to be accounted for when analysing the data. The results presented here contradict these findings, since we show that non-thermal trapping is not important for bulk studies of thermal vacancies, even if resonances exist in the trapping rate above thermal energy [13, 14].

The slowing down and thermalization of positrons have been studied theoretically by many authors, e.g. [15–20]. The results show that electron scattering is the dominant energy loss mechanism for positron energies above about 1 eV, while acoustic phonon scattering becomes increasingly important as the positron approaches thermal energies. In most cases [15, 16, 18, 20] the slowing-down processes have been described in terms of averaged scattering parameters such as the mean free path and the average energy loss rate. This approach ignores the fact that the positrons have an energy distribution of non-negligible width, which leads to considerably higher energy loss rates compared to when all positrons are assumed to have a single energy at a given time [17]. Only in the case where phonon scattering is neglected, i.e. electron scattering only, has the slowing down been followed in detail by calculations of the time-dependent momentum distribution from the Boltzmann equation [17]. We go beyond earlier treatment in the present work by including both electron and phonon scattering in a formulation based on the Boltzmann equation.

Our theory also allows us to calculate the momentum distribution from which the positrons annihilate, including the contribution of non-thermal annihilation. In simple metals this distribution can be deduced experimentally from ACAR (angular correlation of annihilation radiation) measurements [21, 22]. These experiments provide evidence for the rapid thermalization of positrons, since the distribution of annihilating positrons is observed to be a thermal distribution within experimental accuracy even for temperatures as low as 10 K. This result is confirmed by our calculations. We do predict significant non-thermal annihilation at very low temperatures, but the finite momentum resolution of ACAR means that the resulting difference between the annihilation distribution and the thermal distribution is difficult to detect.

We describe the Boltzmann equation, scattering mechanisms and how we find the steady-state and time-dependent distributions in section 2, present and discuss the results in section 3 and go further into the implications of our results in section 4. Section 5 contains a brief set of conclusions. The asymptotic behaviour at long times is discussed briefly in the appendix.

2. Theory

2.1. Boltzmann equation and scattering mechanisms

The thermalization of positrons is studied by solving the Boltzmann equation for the positron momentum distribution $n(\boldsymbol{p}, t)$ in a homogeneous medium [17]:

$$\frac{\mathrm{d}}{\mathrm{d}t} n(\boldsymbol{p}, t) = \int \mathrm{d}^3 q \, [R(\boldsymbol{q}, \boldsymbol{p}) n(\boldsymbol{q}, t) - R(\boldsymbol{p}, \boldsymbol{q}) n(\boldsymbol{p}, t)] - [\lambda + \kappa(\boldsymbol{p})] n(\boldsymbol{p}, t) + n_i(\boldsymbol{p}, t). \quad (1)$$

Here $R(\boldsymbol{p}, \boldsymbol{q})\, \mathrm{d}^3 q$ denotes the transition rate from momentum state $\hbar \boldsymbol{p}$ to momenta in the

volume $\hbar^3\,\mathrm{d}^3q$ around $\hbar\boldsymbol{q}$; λ is the annihilation rate, which is assumed to be independent of momentum since we consider only fairly low momenta [23]; and $\kappa(\boldsymbol{p})$ is the momentum-dependent trapping rate into defects. The term $n_i(\boldsymbol{p}, t)$ represents the external source of positrons. If more than one type of trap is present, κ is a sum of individual trapping rates κ_i: $\kappa(p) = \Sigma_i \kappa_i(p)$. We will in all cases assume that no detrapping occurs, i.e. trapped positrons are removed from the system and annihilate from a trapped state. It is also assumed that there is no explicit time dependence of the trapping rates, which has been shown by McMullen [24] to be a reasonable assumption for vacancies for which the rate-limiting process is the quantum-mechanical transition from the delocalized to the trapped state. This assumption no longer holds if trapping is also limited by the diffusion of positrons to the traps [25, 26], as appears to be the case for large voids [27, 28].

We will assume that the distribution is isotropic, $n(\boldsymbol{p}, t) \equiv n(p, t)$, and define the distribution of momentum magnitudes $f(p, t)$ and the related $f_i(p, t)$ from

$$\begin{aligned} f(p, t) &\equiv p^2 n(p, t) \\ f_i(p, t) &\equiv p^2 n_i(p, t). \end{aligned} \tag{2}$$

Equation (1) can then be simplified to

$$\frac{\mathrm{d}}{\mathrm{d}t} f(p, t) = \int \mathrm{d}q\, K(q, p) f(q, t) - H(p) f(p, t) + f_i(p, t). \tag{3}$$

The kernel $K(q, p)$, which accounts for scattering of positrons from states in the interval $\hbar\,\mathrm{d}q$ around $\hbar q$ into state $\hbar p$, is given by

$$K(q, p) = p^2 \int \mathrm{d}\theta_q \sin\theta_q \int \mathrm{d}\varphi_q\, R(\boldsymbol{q}, \boldsymbol{p}) \tag{4}$$

where θ_q and φ_q are the directional angles of $\boldsymbol{q}$. The function H is the rate of loss of positrons from state p due to scattering, annihilation and trapping:

$$H(p) = H_{\mathrm{sc}}(p) + \lambda + \kappa(p) \tag{5}$$

with the scattering contribution given by

$$H_{\mathrm{sc}}(p) = \int \mathrm{d}^3q\, R(\boldsymbol{p}, \boldsymbol{q}). \tag{6}$$

Since the slowing down of positrons to energies of the order of 10 eV is extremely rapid [16–18, 20] we need here only consider the processes at low positron energies. The dominant scattering mechanisms for positrons below 10 eV are acoustic phonon and conduction electron scattering [20]. Thus,

$$R(\boldsymbol{p}, \boldsymbol{q}) = R_{\mathrm{ph}}(\boldsymbol{p}, \boldsymbol{q}) + R_{\mathrm{el}}(\boldsymbol{p}, \boldsymbol{q}). \tag{7}$$

Phonon scattering is included in a Debye model [16, 20]:

$$\begin{aligned} R_{\mathrm{ph}}(q, p) = \frac{\gamma^2}{4\pi^2} k\{&[\eta_{\mathrm{B}}(\hbar c_{\mathrm{s}} k) + 1]\delta(E_+(\boldsymbol{k} + \boldsymbol{p}) - E_+(\boldsymbol{p}) - \hbar c_{\mathrm{s}} k)\Theta(\omega_{\mathrm{D}} - c_{\mathrm{s}} k) \\ &+ \eta_{\mathrm{B}}(\hbar c_{\mathrm{s}} k)\delta(E_+(\boldsymbol{k} + \boldsymbol{p}) - E_+(\boldsymbol{p}) + \hbar c_{\mathrm{s}} k)\Theta(\omega_{\mathrm{D}} - c_{\mathrm{s}} k)\} \end{aligned} \tag{8}$$

where $\boldsymbol{k} = \boldsymbol{p} - \boldsymbol{q}$, c_{s} is the sound velocity in the medium, ω_{D} is the Debye frequency, $\eta_{\mathrm{B}}(E) = [\exp(E/k_{\mathrm{B}}T) - 1]^{-1}$ is the Bose–Einstein distribution function, in which k_{B} is the Boltzmann constant and T the absolute temperature, m^* is the effective positron mass entering the nearly-free-particle expression assumed for the positron energy,

$E_+(\boldsymbol{p}) = \hbar^2 p^2/2m^*$, and γ^2 is the square of the positron–phonon coupling constant. We use a deformation potential approximation $\gamma^2 = E_{\mathrm{def}}^2/(2NMc_s)$, where E_{def} is the positron deformation potential, N the atomic density and M the atomic mass of the solid. Equation (8) represents the positron–phonon interaction to lowest order in the phonon–positron coupling. McMullen [29] has demonstrated the validity of this approximation by comparing positron self-energies calculated with the lowest-order formula and a strong-coupling approach. The first term in equation (8) describes phonon emission and the second term phonon absorption.

Conduction electron scattering is included in the random-phase approximation (RPA) assuming a free-electron gas. Since we are interested in low positron energies and thus low energy and momentum transfers in each scattering event, we take the low-energy and low-momentum limit of the RPA also used by Woll and Carbotte [17]:

$$R_{\mathrm{el}}(\boldsymbol{q},\boldsymbol{p}) = \frac{1}{\hbar\pi}\left(\frac{e^2 a_0}{16\pi^2\varepsilon_0 k_F}\right)^2 \int \mathrm{d}^3k\, \delta(E_-(\boldsymbol{k}+\boldsymbol{q}-\boldsymbol{p}) + E_+(\boldsymbol{p}) - E_-(\boldsymbol{k}) - E_+(\boldsymbol{q})) \times [1 - \eta_F(E_-(\boldsymbol{k}+\boldsymbol{q}-\boldsymbol{p}))]\eta_F(E_-(\boldsymbol{k})) \tag{9}$$

where e is the electron charge, a_0 the Bohr radius, $\hbar k_F$ the Fermi momentum, ε_0 the vacuum permeability, $E_-(\boldsymbol{k}) = \hbar^2 k^2/2m$ the electron energy with m being the electron mass, and η_F the Fermi function $\eta_F(E) = \{\exp[(E - E_F)/k_B T] + 1\}^{-1}$ where E_F is the Fermi energy. It is well known that the RPA underestimates the positron–electron correlation at low energies, see e.g. [30]. Thus, equation (9) may underestimate the true scattering rates, see also [31, 32]. However, as will be demonstrated below, the most important energy region in the context of thermalization and non-thermal trapping is below 1 eV where phonon scattering dominates. The primary role of the electron scattering is to slow the positron down to about 1 eV extremely rapidly, and quantitative inaccuracies in the description of this process give rise to only minor changes in the results to be presented in section 3.

With the scattering rates described by equations (8) and (9) we have the following expressions for the scattering terms in the Boltzmann equation (3):

$$\begin{aligned}\int \mathrm{d}q\, K(q,p) f(q,t) = {} & \frac{\pi m e^4 a_0^2}{8m^* E_F (4\pi\varepsilon_0)^2 \hbar} \\ & \times \left(\frac{1}{p}\int_0^p \mathrm{d}q (p^2 - q^2)\frac{\exp[\hbar^2(q^2-p^2)/2m^*k_BT]p^2 f(q,t)}{1 - \exp[\hbar^2(q^2-p^2)/2m^*k_BT]}\right. \\ & \left. + \int_p^\infty \mathrm{d}q \frac{p^2 - q^2}{q}\frac{p^2 f(q,t)}{1 - \exp[\hbar^2(p^2-q^2)/2m^*k_BT]}\right) + \frac{\gamma^2 m^*}{2\pi} \\ & \times \left[p\int_{a_1}^{b_1} \mathrm{d}k \frac{f((p^2 + 2m^*c_s k/\hbar)^{1/2}, t)}{p^2 + 2m^*c_s k/\hbar} k^2 \left(1 + \frac{1}{\exp(\hbar c_s k/k_B T) - 1}\right)\right. \\ & \left. + p\int_{a_2}^{b_2} \mathrm{d}k \frac{f((p^2 - 2m^*c_s k/\hbar)^{1/2}, t)}{p^2 - 2m^*c_s k/\hbar}\frac{k^2}{\exp(\hbar c_s k/k_B T) - 1}\right]\end{aligned} \tag{10}$$

and

$$\begin{aligned}H_{\mathrm{sc}}(p) = {} & \frac{\pi m e^4 a_0^2}{8m^* E_F (4\pi\varepsilon_0)^2 \hbar}\left(\frac{1}{p}\int_0^p \mathrm{d}q\,(p^2 - q^2)\frac{q^2}{1 - \exp[\hbar^2(q^2-p^2)/2m^*k_BT]}\right. \\ & \left. + \int_p^\infty \mathrm{d}p\, q(p^2 - q^2)\frac{\exp[\hbar^2(p^2-q^2)/2m^*k_BT]}{1 - \exp[\hbar^2(p^2-q^2)/2m^*k_BT]}\right)\end{aligned}$$

$$+\frac{\gamma^2 m^*}{2\pi}\frac{1}{p}\left[\int_{a_1}^{b_1} \mathrm{d}k \frac{k^2}{\exp(\hbar c_s k/k_B T)-1}\right.$$

$$\left.+\int_{a_2}^{b_2} \mathrm{d}k\, k^2\left(1+\frac{1}{\exp(\hbar c_s k/k_B T)-1}\right)\right]. \tag{11}$$

Here the integration limits in the phonon scattering integrals are

$$a_1 = \max(0, 2(m^* c_s/\hbar - p))$$

$$b_1 = \min(\omega_D/c_s, 2(m^* c_s/\hbar + p))$$

$$a_2 = 0$$

$$b_2 = \min[\omega_D/c_s, \max(0, 2(p - m^* c_s/\hbar))].$$

As in [17] we neglect terms proportional to $\exp(-E_F/k_B T)$ in the electron scattering calculation.

We have solved the Boltzmann equation, equation (3), for the cases where the positron source term, $f_i(p, t)$, is (i) a delta function in time and (ii) independent of time. These will be described in the following two subsections. In both cases the equation can be solved without any additional approximations. Thus, apart from the necessarily approximate description of the scattering rates, our solutions of the Boltzmann equation are exact to within the numerical accuracy.

The parameters used in the calculations are for aluminium: $E_F = 11.7\,\mathrm{eV}$, $c_s = 6.4 \times 10^3\,\mathrm{m\,s^{-1}}$ [33], $\omega_D = 5.2 \times 10^{13}\,\mathrm{s^{-1}}$ (corresponding to a Debye temperature $\Theta_D = \hbar\omega_D/k_B = 394\,\mathrm{K}$) [34], $N = 6.0 \times 10^{28}\,\mathrm{m^{-3}}$, $M = 27 m_p$ (m_p is the proton mass), $E_{def} = -8.6\,\mathrm{eV}$ [35] and $\lambda = 6.163 \times 10^9\,\mathrm{s^{-1}}$ [7]. The effective positron mass m^* is assumed equal to the electron mass m, but results for $m^* > m$ are briefly discussed at the end of section 3.

2.2. *Time-dependent momentum distributions*

If f_i is a delta function in time, i.e.

$$f_i(p, t) = f_1(p)\delta(t) \tag{12}$$

equation (3) describes the time development of the positron momentum distribution from the initial distribution $f_1(p)$. For zero trapping, $\kappa(p) = 0$, the solution can be written in the form [17]

$$f(p, t) = \exp(-\lambda t) g(p, t) \tag{13}$$

where $g(p, t)$ satisfies

$$\frac{\mathrm{d}}{\mathrm{d}t} g(p, t) = \int \mathrm{d}q\, K(q, p) g(q, t) - H_{sc}(p) g(p, t) \tag{14}$$

with the initial condition

$$g(p, 0) = f_1(p). \tag{15}$$

The stationary solution of this equation corresponding to large values of t is the Maxwell–Boltzmann distribution at the temperature of the system. Equation (14) was integrated numerically using a fourth-order Runge–Kutta method [36] from a given initial distribution. The calculations were performed on a mesh of typically 300 points, which was

updated regularly as t progressed to make the mesh cover only regions where g is significantly different from zero. The size of each time step in the Runge–Kutta integration was adjusted to give a relative accuracy of g better than 10^{-3} at all momenta. The calculations presented in section 3.1 required 500–800 time steps with this accuracy.

Our calculations are similar to those of Woll and Carbotte [17] but we take into account both electron and phonon scattering. In a test calculation with electron scattering only and parameters identical to those of Woll and Carbotte [17] we obtained results in agreement with theirs.

2.3. Steady-state momentum distributions

When f_i is independent of t, $f_i(p, t) = f_i(p)$, we get a steady state with $\mathrm{d}f/\mathrm{d}t = 0$. Equation (3) thus reduces to an integral equation for $f(p) \equiv f(p, t)$:

$$\int \mathrm{d}q\, K(q, p) f(q) - H(p) f(p) + f_i(p) = 0. \tag{16}$$

We have solved this equation iteratively, starting from an initial guess $f_{[0]}(p)$, and obtaining the $(n+1)$th iteration $f_{[n+1]}$ from $f_{[n]}$ using the prescription

$$f_{[n+1]}(p) = A \frac{\mu_n}{H(p)} \left(\int \mathrm{d}q\, K(q, p) f_{[n]}(q) + f_i(p) \right) + (1 - A) f_{[n]}(p) \tag{17}$$

where the normalization factor μ_n is evaluated from $f_{[n]}$ using the equation

$$\mu_n = \int \mathrm{d}p\, f_i(p) \Big/ \left[\int \mathrm{d}p \left(\int \mathrm{d}q\, K(q, p) f_{[n]}(q) - H(p) f_{[n]}(p) \right) \right] \tag{18}$$

which enforces particle conservation. The feedback parameter A in equation (17) controls how large a fraction of the new estimate for f is mixed into the previous estimate. It has been shown that the iterative prescription of equation (17) converges to the correct solution of equation (16) [37]. The method of [37] did not incorporate the update of the normalization factor μ_n, equation (18), but we found that it stabilized the convergence. We also found that setting $A = 1$ in some cases led to a divergence of the iteration, presumably due to numerical inaccuracies. Setting $A < 1$ is equivalent to including a 'self-scattering' term in the Boltzmann equation, i.e. a fictitious scattering process which leaves the positron state unaltered, see [37, 38]. We used a value for A close to 1, typically 0.8. We repeated the iterations until μ_n was equal to its asymptotic value of 1.0 to within 1 ppm. At this point all other parameters, such as the average energy and trapping probabilities, were well converged. Convergence normally required a few hundred iterations on a typical mesh of 500 momentum points.

The solution of equation (16), $f(p)$, corresponds to the momentum distribution from which the positrons annihilate. This is, in the case of no trapping, related to the time-dependent momentum distribution $g(p, t)$ through the relation

$$f(p) = \int \mathrm{d}t \exp(-\lambda t) g(p, t) \tag{19}$$

which was confirmed numerically. When traps are present, the influence of trapping on the momentum distribution [39] is automatically incorporated.

The distribution of implanted positrons f_i was always normalized to correspond to one positron introduced per atomic unit of time (which is 2.42×10^{-17} s). This normalization determines the absolute values of $f(p)$ via

$$\int \mathrm{d}p\ [\lambda + \kappa(p)]f(p) = \int \mathrm{d}p\, f_i(p) \tag{20}$$

but does not affect any of the other calculated parameters. The integral of f,

$$\int \mathrm{d}p\, f(p)$$

corresponds to the total number of positrons present in the system at a given time and is determined through equation (20) by the influx of positrons and by the annihilation and trapping rates. Equation (20) is always obeyed by the solution to equation (16). However, numerical errors in the calculation of the scattering rates give rise to a difference between the right- and left-hand sides of the equation. Increasing the mesh point density decreases this difference. Accordingly, the number of mesh points was always chosen large enough for equation (20) to be obeyed to within an accuracy better than 1%.

The fraction of positrons trapped into traps of type i before annihilation is given by

$$N_i = \bar{\kappa}_i \Big/ \Big(\lambda + \sum_j \bar{\kappa}_j\Big) \tag{21}$$

where

$$\bar{\kappa}_i = \int \mathrm{d}p\, \kappa_i(p) f(p) \Big/ \Big(\int \mathrm{d}p\, f(p)\Big). \tag{22}$$

N_i corresponds to the relative intensity of the component due to traps of type i in an ACAR or Doppler broadening spectrum. It is less straightforward to calculate the corresponding intensities in lifetime spectra. If κ depends on p, it will vary with time during the thermalization of the positron, which means that the lifetime spectrum in general will not be a sum of exponentials like that predicted by the simple trapping model in which constant trapping rates are assumed [40]. However, the deviations from this shape may not be detectable in actual lifetime measurements and the spectrum may be described, within statistical accuracy, by a sum of exponential components. One can obtain an estimate of the relative intensities I_i of the components corresponding to trapped positrons by using the standard trapping model result [40] but using the $\bar{\kappa}_i$ values from equation (22) for the individual trapping rates:

$$I_i = \bar{\kappa}_i \Big/ \Big(\lambda - \lambda_i + \sum_j \bar{\kappa}_j\Big) \tag{23}$$

where λ_i is the positron annihilation rate in traps of type i. From these intensities we can estimate the mean lifetime:

$$\tau_{\mathrm{m}} = \Big(1 - \sum_j I_j\Big) \Big/ \Big(\lambda - \sum_j \bar{\kappa}_j\Big) + \sum_j \frac{I_j}{\bar{\kappa}_j}. \tag{24}$$

We expect equations (23) and (24) to be reasonably accurate since, as will appear from the next section, the deviations from the simple trapping model results are very small in all cases considered in the present paper.

3. Results

3.1. Time-dependent momentum distributions

Figure 1 shows a series of positron momentum distributions $g(p, t)$ at different times calculated from equation (14) with both phonon and electron scattering active. The

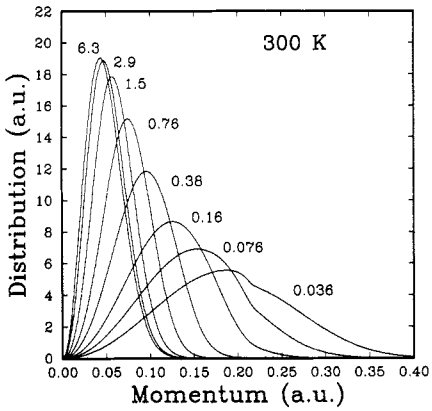

Figure 1. Positron momentum distributions in Al at 300 K. The time after implantation in picoseconds is indicated for each curve. The distributions were obtained by solving the Boltzmann equation, equation (14), with both phonon and electron scattering included.

initial distribution $f_1(p)$ was chosen as a narrow Gaussian centred at $p = 0.857$ au corresponding to an average energy of 10 eV. However, as shown by Woll and Carbotte [17], all memory of the starting distribution is rapidly lost as the scattering takes effect, and the distributions when the positrons approach thermalization are independent of the choice of $f_1(p)$. The distribution shown in figure 1 all correspond to the regime where the effects of the initial distribution are no longer discernible. The distributions converge towards a thermal Maxwell–Boltzmann (MB) distribution as time increases, and the curve for $t = 6.3$ ps is virtually indistinguishable from the MB curve. It is clear from the figure that most of the time is spent with a distribution very close to the thermal distribution. The kinks observed in the curves at $p = 0.213$ au, which is half the Debye momentum, $\hbar k_D = \omega_D/c_s$, reflects the change in the behaviour of the upper limits of the phonon scattering integrals in equations (10) and (11) near this value of p.

Figure 2 shows the average energy of the positrons as a function of time, evaluated from the momentum distributions:

$$\bar{E}(t) = \int \mathrm{d}p\, (\hbar^2 p^2/2m^*) g(p, t). \tag{25}$$

Panel (*a*) of the figure shows results calculated with both phonon and electron scattering for different temperatures T. It is seen that $\bar{E}$ for different values of T is the same down to energies of about 0.3 eV, after which it approaches thermal energies, $E_{th} = \frac{3}{2}k_B T$. The dotted lines in the figure connect points on the curves corresponding to $\bar{E} = 1.1 \times E_{th}$, $1.01 \times E_{th}$ and $1.001 \times E_{th}$, respectively. The corresponding times are tabulated in table 1. Since $\bar{E}$ decreases asymptotically towards E_{th} it is not possible to define a unique thermalization time, but the results in table 1 indicate how long it takes to reach near-thermal energies. The approach of $\bar{E}$ to E_{th} is very close to exponential in the range from $2E_{th}$ to E_{th}: $\bar{E}(t) - E_{th} = \text{constant} \times \exp(-t/t_E)$. This result is discussed in more detail in the appendix. The energy relaxation times t_E at different temperatures are given in table 1. Note that the energy relaxation times are much higher than the scattering times (the inverse of the scattering rates), which are of the order of 10^{-14} s [20]. This is because the small energy transfer in each positron–phonon scattering event means that many scattering events are required to reduce the positron energy significantly.

Our calculations confirm the importance of phonon scattering in the final stages of thermalization [16, 18, 20]. In figure 2(*b*) $\bar{E}$ is compared for calculations with electron scattering only and with both electron and phonon scattering. The energy loss below about 1 eV is seen to be dominated by the phonon scattering.

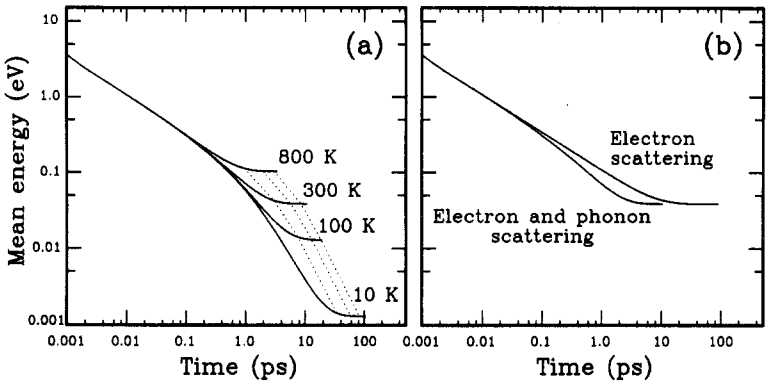

Figure 2. Mean energies $\bar{E}$ as a function of time after implanation for positrons slowing down in Al: (*a*) at different temperatures with both phonon and electron scattering included; and (*b*) at 300 K for either electron scattering only or both phonon and electron scattering. The dotted lines in (*a*) connect points on the curves corresponding to $\bar{E} = 1.1 \times E_{th}$, $1.01 \times E_{th}$, and $1.001 \times E_{th}$, respectively.

Table 1. The times $t_{1.1}$, $t_{1.01}$ and $t_{1.001}$ taken to reach mean energies $1.1 \times E_{th}$, $1.01 \times E_{th}$ and $1.001 \times E_{th}$, respectively, for positrons slowing down at different temperatures. E_{th} is the thermal energy $\frac{3}{2}k_BT$. Also shown is the relaxation time t_E corresponding to the exponential approach of the mean energy to E_{th}.

	Temperature (K)			
	10	100	300	800
$t_{1.1}$ (ps)	34.6	7.4	3.01	0.95
$t_{1.01}$ (ps)	58.7	12.9	5.65	1.94
$t_{1.001}$ (ps)	83.5	18.4	8.38	2.98
t_E (ps)	10.5	2.4	1.2	0.44

The rate of change of the mean energy $d\bar{E}/dt$, obtained by numerical differentiation of the results for $\bar{E}(t)$ shown in figure 2, is plotted as a function of the mean energy $\bar{E}$ in figure 3. Panel (*b*) gives $d\bar{E}/dt$ at different temperatures while panel (*a*) compares $d\bar{E}/dt$ to dE/dt defined by

$$\frac{dE}{dt} = \int d^3q \frac{\hbar^2(p^2 - q^2)}{2m^*} R(\boldsymbol{p}, \boldsymbol{q}). \tag{26}$$

This quantity, which should not be confused with $d\bar{E}/dt$, is the average energy loss rate for a positron at a given momentum p. There are two marked differences between the two curves in figure 3(*a*). Firstly, dE/dt approaches zero at $E = 2k_BT$ while $d\bar{E}/dt$ goes to zero at the true thermal energy $\frac{3}{2}k_BT$; and, secondly, $d\bar{E}/dt$ lies significantly above dE/dt at all energies. Both effects have been pointed out in earlier work [16, 17, 20]. When electron scattering is dominant, $d\bar{E}/dt$ is a factor of nearly 3 higher than dE/dt [17], while the relative difference is smaller but still significant in the low-energy region dominated by phonon scattering.

The distinction between dE/dt and $d\bar{E}/dt$ is important in studies of positron thermalization and non-thermal trapping effects. Studies of these effects have so far mostly

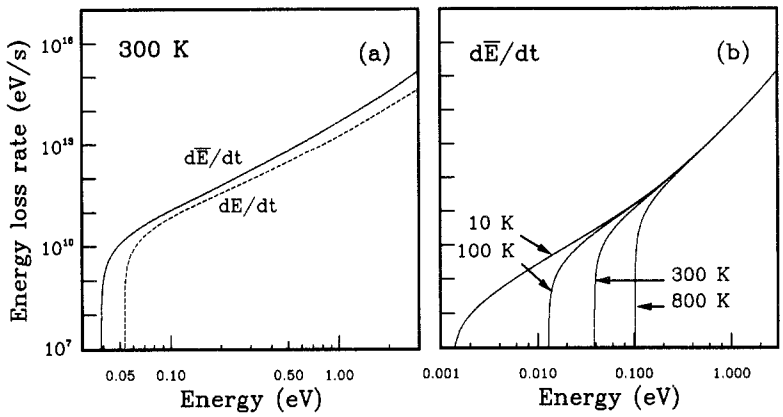

Figure 3. The time derivative of the mean energy $d\bar{E}/dt$ plotted as a function of the mean energy $\bar{E}$. Panel (*a*) compares $d\bar{E}/dt$ for positrons thermalizing at 300 K with the average energy loss rate dE/dt, calculated from equation (26), plotted as a function of $E = \hbar^2p^2/2m^*$. Panel (*b*) shows $d\bar{E}/dt$ for four different temperatures.

been based on calculations of the positron slowing down by integrating dE/dt [6, 16, 20, 41]. This corresponds to assuming the positron momentum distribution to be a delta function (in momentum) at all times. Figure 3 shows that this underestimates the slowing-down rate and thus overestimates the thermalization time, and only if the statistical nature of the energy loss processes is considered does one obtain thermalization of the positrons at the correct energy. This emphasizes the point made in the introduction that the full statistical description of the slowing-down process is necessary for accurate calculations of positron thermalization effects.

The values for dE/dt (as distinct from $d\bar{E}/dt$) are in excellent agreement with those of Nieminen and Oliva [20] who used the full RPA to calculate the positron–electron scattering. Hence our use of the low-energy and low-momentum limit of the RPA is adequate for the present work.

3.2. Steady-state momentum distributions

Below we present examples of calculated steady-state momentum distributions with and without trapping and at different temperatures. In all cases the source distribution $f_i(p)$ is a narrow Gaussian corresponding to an energy of 3 eV but the distributions in the momentum range shown in the figures are not influenced by the choice of f_i as long as the initial mean energy is higher than ~2 eV.

The steady-state distribution in the absence of trapping is compared to the Maxwell–Boltzmann distribution

$$f_{MB}(p) = Cp^2 \exp(\hbar^2p^2/2m^*k_BT) \tag{27}$$

(C is a normalization constant) in figure 4. Results are shown for temperatures 10 and 300 K. The figure shows that $f(p)$ consists of a MB-like distribution with a tail of low intensity extending to high momenta. The tail represents positrons annihilating before thermalization. It is not possible to divide the distribution uniquely into thermal and non-thermal positrons. Attempts to subtract the MB contribution from f gave quite different results depending on the range used to match f and the MB distribution when determining the relative intensity of the MB distribution. This is directly related to the

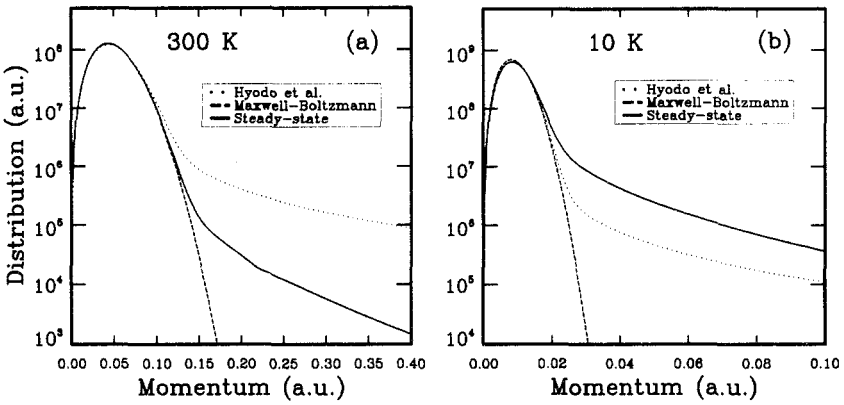

Figure 4. Steady-state positron momentum distributions calculated from the Boltzmann equation at $T = 300$ K (*a*) and $T = 10$ K (*b*), in both cases without any defect trapping. Also shown are the thermal Maxwell–Boltzmann distributions and the momentum distributions calculated by Hyodo *et al* [42], which include the effects of positron–phonon interactions. The curves in each panel are normalized to have the same total area.

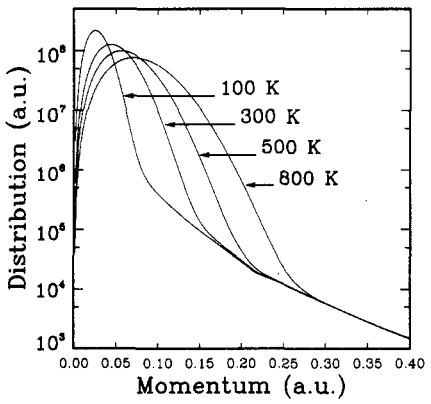

Figure 5. Steady-state momentum distribution for different temperatures in the absence of defect trapping.

fact mentioned above that there is no unique thermalization time since the positron momentum distribution reaches the MB distribution only in the asymptotic limit $t \rightarrow \infty$. The kink in f at $p = 0.213$ au reflects, like those seen in figure 1, the change in the phonon scattering near $p = k_D/2$.

The temperature dependence of $f(p)$ is illustrated in figure 5. It is seen that the tail is approximately independent of T but the fraction of positrons in the tail increases with decreasing temperature. The mean energy $\bar{E}$ of the steady-state distribution,

$$\bar{E} = \int \mathrm{d}p(\hbar^2 p^2/2m^*) f(p) \tag{28}$$

is shown as a function of temperature in figure 6. At high temperatures $\bar{E}$ is extremely close to the thermal energy E_{th} but the relative difference between the two increases with decreasing T. However, only at very low temperatures, below 50 K, is $\bar{E}$ substantially higher than E_{th}. As T approaches zero, $\bar{E}$ converges towards a minimum of about 2×10^{-3} eV corresponding to an effective temperature of 15 K. These results are in accordance with the ACAR results [21] within the experimental uncertainty and confirm

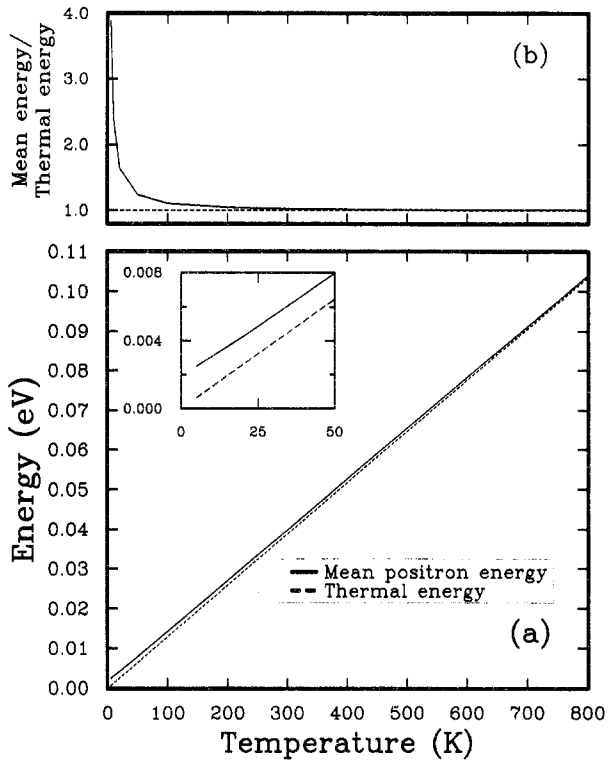

Figure 6. (*a*) Mean positron energies calculated from the steady-state momentum distributions at different temperatures assuming no trapping. Panel (*a*) also shows the thermal energy $\frac{3}{2}k_BT$. The insert is a magnification of the low-temperature region. (*b*) The ratio of the mean positron energy and the thermal energy.

the conclusion of [21] that the positrons annihilate from a distribution close to a MB distribution even at low temperatures. Because of the finite angular resolution in ACAR the discrepancy between $\bar{E}$ and E_{th} at low temperatures is difficult to detect since the absolute difference between the two is very small.

Mechanisms other than non-thermal annihilation can give rise to tails in the positron momentum distribution. For example, the positron–phonon interaction gives rise to a p^{-2} tail [42, 43]. The momentum distributions for thermal positrons at 10 and 300 K, taking into account the dressing of the positron by phonons according to equation (a3) of [42], are shown in figure 4. The p^{-2} tail at 300 K has a significantly higher intensity than the tail due to non-thermals. At higher temperatures the difference between the two tails is greater than at 300 K while the non-thermal tail becomes more prominent than that due to the positron–phonon interaction at low temperatures below ~100 K, as demonstrated by the $T = 10$ K results in figure 4(*b*). The presence of the p^{-2} tail means that the non-thermal tail will be difficult to observe directly by bulk positron techniques such as ACAR.

Hyodo *et al* [22] have made a detailed analysis of ACAR spectra for potassium at temperatures above 91 K using the theoretical positron momentum distribution of [42] including the p^{-2} tail. We have confirmed that this p^{-2} tail is considerably larger than the non-thermal tail at all temperatures considered by Hyodo *et al* by solving the Boltzmann equation for potassium. Thus, the neglect of non-thermal effects in [22] is justified.

The effects of trapping on the steady-state distribution are illustrated in figure 7. The trapping rate κ is given by $\kappa = \mu C$ where C is the defect concentration and μ is the

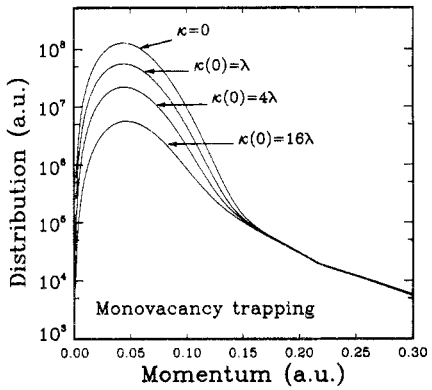

Figure 7. Steady-state momentum distributions at 300 K when monovacancies are present. Results are shown for different total trapping rates, corresponding to different vacancy concentrations. The value of the trapping rate at zero momentum $\kappa(0)$, which fixes the absolute values of the momentum-dependent trapping rates, is indicated for each curve; λ is the bulk annihilation rate.

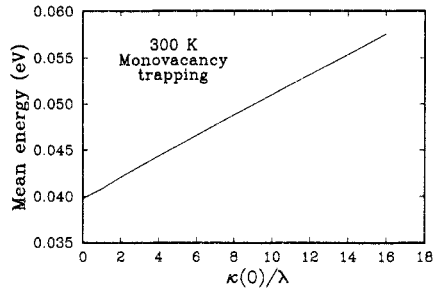

Figure 8. The mean positron energy calculated from the steady-state momentum distribution at 300 K when trapping into monovacancies occurs. The energy is shown as a function of the trapping rate at zero momentum, which fixes the absolute values of the momentum-dependent trapping rates; λ is the bulk annihilation rate.

specific trapping rate. We have used the (momentum-dependent) specific trapping rate μ_{1V} calculated by Puska and Manninen [14] for monovacancies in Al. This trapping rate has a strong maximum at a positron energy of about 2 eV due to resonance trapping. Figure 7 shows results for three different total trapping rates corresponding to different defect concentrations. The presence of traps leaves the tail of the momentum distribution essentially unaffected but depletes the thermal part due to the removal of positrons by trapping. As shown in figure 8, this leads to an increase in $\bar{E}$ with increasing trapping rate.

Figure 9 demonstrates the effects of non-thermal trapping on the trapping probability by comparing the results calculated from equation (21) with those obtained for thermal trapping, i.e. the trapping probability for positrons with a thermal Maxwell–Boltzmann momentum distribution. The figure shows the variation with temperature for a given trapping rate. The relative enhancement of the trapping due to non-thermal trapping is in all cases only a fraction of a per cent. Similar results were found for all systems that produced the results in figure 8, i.e. varying the trapping rate at a fixed temperature. The results lead to the immediate conclusion that non-thermal trapping has very little effect on the trapping probability for monovacancies. This result is valid not only for the trapping probability but also for the lifetime intensity, calculated from equation (23). The results show that, although the trapping rates for non-thermal energies are significantly higher than thermal trapping rates, the positron thermalization is too fast for non-thermal trapping to have an appreciable effect on the measurable parameters.

This conclusion holds even when a trapping resonance exists at near-thermal energies. This is demonstrated by the results calculated for the trapping probability into divacancies shown in figure 10 (a defect population consisting of divacancies only is probably unlikely in reality but it provides a convenient example of a trapping rate with a low-energy resonance). We have used the specific trapping rate μ_{2V} from [14], which has a resonance peak around 0.1 eV and exhibits a much larger energy variation in the

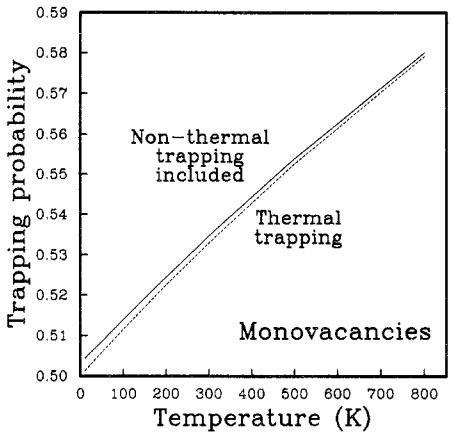

Figure 9. The probability of positrons being trapped by monovacancies as a function of temperature. The vacancy concentration is chosen to make the trapping rate at zero momentum equal to the bulk annihilation rate. With a specific trapping rate of $\mu_{1V}(0) = 3.8 \times 10^{14}\ s^{-1}$ [14] this means a concentration of 16 ppm. The momentum dependence of the trapping rate is taken from [14]. The figure shows both the results calculated from the Boltzmann equation, which includes non-thermal effects, and the result for thermal trapping only, i.e. the result obtained by averaging the trapping rate over the thermal Maxwell–Boltzmann distribution.

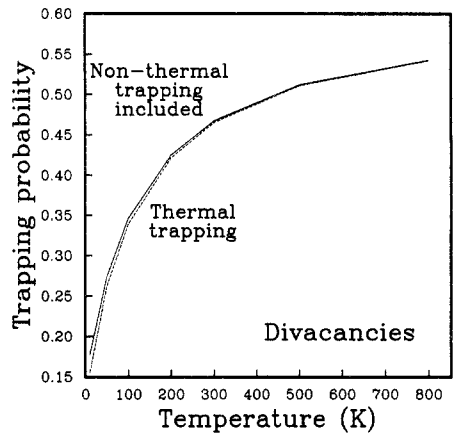

Figure 10. The probability of positrons being trapped by divacancies as a function of temperature. The divacancy concentration is 1.7 ppm assuming a specific trapping rate $\mu_{2V}(0) = 4.9 \times 10^{14}\ s^{-1}$ [14]. The momentum dependence of the trapping rate is taken from [14]. The figure shows both the result calculated from the Boltzmann equation, which includes non-thermal effects, and the result for thermal trapping only.

thermal energy range than μ_{1V}. Despite this fact the figure shows that non-thermal trapping is unimportant even in this case.

We have also calculated the effects of non-thermal trapping on positron studies of thermal defects. Two different choices have been employed for the defect populations. The results of Fluss *et al* [44] indicate a significant contribution of divacancies to the trapping rate at high temperatures. However, the results of Jackman *et al* [7] appear to contradict this finding, and theoretical estimates of the binding energy of divacancies in Al [45] suggest that divacancies are only weakly bound and therefore unlikely to exist in significant concentrations at high temperatures. Because of this controversy we have performed calculations when both mono- and divacancies are included and for a defect population consisting of monovacancies alone. The concentrations were evaluated as

$$C_{nV}(T) = \exp(S_{nV}/k_B)\exp(-H_{nV}/k_B T) \tag{29}$$

with $n = 1$ and $n = 2$ denoting mono- and divacancies, respectively. In the first set of calculations we used formation enthalpies of $H_{1V} = 0.66$ eV and $H_{2V} = 1.02$ eV [44] and entropies $S_{1V}/k_B = 1.3$ [44] and $S_{2V}/k_B = 3.8$. We have adjusted S_{2V} to correspond to $\mu_{2V}/\mu_{1V} = 10$, approximately the value predicted at high temperatures by Puska and Manninen [14]. Fluss *et al* [44] obtained $S_{2V}/k_B = 5.6$ assuming $\mu_{2V}/\mu_{1V} = 2$. None of the qualitative conclusions in the following are affected by which of the two values of S_{2V}/k_B is used. In the second set of calculations we chose $H_{1V} = 0.71$ eV and $S_{1V}/k_B = 1.23$ according to the results of Jackman *et al* [7], and no divacancies were included.

Table 2 presents the calculated trapping probabilities for thermal defects at different temperatures and compares the probabilities obtained from the full calculation with

Table 2. Trapping probabilities N_1 and N_2 into thermally generated mono- and divacancies, respectively, at different temperatures. Results are given both for purely thermal trapping and from the full calculation using the Boltzmann equation, which includes the effect of non-thermal trapping. Also shown are mean lifetimes τ_m evaluated from equation (24). The top half of the table gives the results when both mono- and divacancies are present [8], while in the bottom half only monovacancies are included [7].

Defect population	T (K)	Full calculation			Thermal trapping		
		N_1 (%)	N_2 (%)	τ_m (ps)	N_1 (%)	N_2 (%)	τ_m (ps)
Mono- and divacancies	500	5.85	0.14	167.6	5.84	0.14	167.6
	600	43.4	4.11	200.8	43.3	4.11	200.8
	700	69.2	17.8	235.5	69.0	17.9	235.4
	800	63.6	33.5	248.2	62.8	34.3	248.3
	900	53.5	43.8	253.6	50.4	48.8	254.5
Monovacancies only	500	1.80			164.4	1.79	164.4
	600	22.8			180.6	22.8	180.5
	700	68.6			215.8	68.5	215.7
	800	90.9			233.0	90.8	232.9
	900	97.1			237.7	97.0	237.6

those obtained without any non-thermal trapping. We also present values for the mean lifetimes calculated from equation (24) assuming $\lambda_1 = 4.167\ \text{ns}^{-1}$ and $\lambda_2 = 3.690\ \text{ns}^{-1}$ [7]. The difference between the two sets of results (full calculation versus thermal trapping) is seen to be extremely small for both choices of defect population. The results thus imply that non-thermal trapping effects do not affect the determination of vacancy formation parameters to any significant degree.

The ACAR results by Hyodo *et al* [42] indicate that m^* for Al is about 1.3 instead of the value of 1 employed in the present calculations. We did additional calculations with $m^* = 1.3$ to confirm that the choice of m^* does not affect any of the conclusions. The difference between $\bar{E}$ and E_{th} was found to be up to 30% lower for $m^* = 1.3$ than for $m^* = 1$, with the values at low temperatures showing the strongest dependence on m^*. Reductions of similar magnitude were also found for the enhancement of the trapping probabilities compared to purely thermal trapping. Thus, setting m^* greater than m would lead to an even smaller influence of non-thermal positrons than indicated by the results presented in the figures and tables.

4. Discussion

The results presented in this paper argue strongly in favour of the use of the conventional trapping model (CTM) for obtaining defect parameters in positron defect studies. Our rationale is that measurable deviations from the CTM will occur only if the trapping rate and/or annihilation rate deviate from the thermal rate for a sufficient fraction of the thermalization period. Because of the asymptotic approach to thermal equilibrium, there is in principle no clear-cut distinction between thermal and non-thermal positrons and in practice we have shown that the positron spends most of the thermalization period with a momentum distribution close to the thermal Maxwell–Boltzmann distribution. We have been able to take this fact into account by calculating the effects of trapping directly from the full positron momentum distribution without an artificial separation of non-thermals from thermals.

The analysis of non-thermal trapping by Warburton and Shulman [5] is consistent with the CTM in the limit where the non-thermal trapping rate is equal to the thermal rate. However, in the paper by Sharma *et al* [9] and some of the later applications and generalizations [6–8, 10–12] it is implicitly assumed that positrons can get trapped but not annihilate during the thermalization period. This assumption leads to predicted departures from the CTM even for energy independent trapping rates, and the consistency with the CTM, referred to above, is no longer present. It also results in an overestimate of the effects of non-thermal trapping, which partially explains why earlier work has predicted a much larger influence of non-thermal trapping than that presented here. Another important difference between the present and earlier work is the positron thermalization is significantly more rapid when using a full description of the time-dependent positron momentum distribution compared to models based on average energy loss rates (see figure 3 and associated discussion above).

Experimental results for a number of metals [7–12] have indicated deviations from the CTM, attributed to trapping of non-thermal positrons, when thermal vacancies act as positron traps. However, these deviations appear not always to be reproducible [46–49], and our results imply that, if the effect is real, explanations other than non-thermal trapping must be considered.

Although the present results indicate that non-thermal effects are unimportant for bulk positron studies of vacancies in metals, it is still possible to envisage situations where non-thermal trapping may play a significant role. Since the energy region immediately above thermal energy is the most important for non-thermal trapping, a large energy variation of the trapping rate at near-thermal energies can lead to non-thermal effects larger than those described above. An example is trapping into large voids at low temperatures for which the thermal trapping rate has been predicted to go to zero as the temperature goes to zero [50], while experimentally a significant fraction of positrons are found to be trapped even at temperatures below 10 K, see, e.g., [27, 28]. Non-thermal trapping is a possible explanation for this apparent discrepancy, as will be discussed in detail in a separate publication [51].

Another example where non-thermal trapping might be significant could be trapping by defects in semiconductors, especially positively charged defects, since the positron has to tunnel through the potential barrier surrounding the defect to get trapped, which leads to a very strong temperature dependence of the trapping rate [52]. Depending on the height of the barrier a significant fraction of positrons may also be trapped at energies at which it is possible to surmount the barrier, which could imply that nearly all trapping into positive defects would be due to non-thermalized positrons.

Non-thermal trapping can also be important if there is a strong sink in the system removing a large fraction of positrons while they are still at non-thermal energies. This situation is encountrered, for example, when positrons are implanted using a low-energy positron beam since the time spent before returning to the sample surface can be short, ~0.1–1 ps, compared to thermalization times. We can simulate the presence of a surface by replacing the true annihilation rate λ by a high effective removal rate λ_{eff}, representing loss of positrons through the surface, in the steady-state Boltzmann equation for positron momentum transport, equation (16). For $\lambda_{\text{eff}} = 10^{13}\ \text{s}^{-1}\ (= 1/(0.1\ \text{ps}))$ we find that about 7% of the positrons get trapped in thermal defects at 850 K (including both mono- and divacancies in the defect population). For thermal positrons only about 3% would be trapped for this value of λ_{eff}. For $\lambda_{\text{eff}} = 10^{12}\ \text{s}^{-1}\ (= 1/(1\ \text{ps}))$ the trapped fraction is about 33%. For thermal positrons about 30% would get trapped. Thus even if the positrons only stay in the sample for 0.1–1 ps and do not have time to thermalize, a substantial

fraction of the positrons may still be trapped, as has been observed experimentally in the positron beam experiments by Nielsen *et al* [53]. To study positron slowing down and trapping near a surface in detail one has to consider the coupled spatial and momentum transport with the proper surface boundary condition [19]. Work is under way to include spatial transport in the Boltzmann equation. We therefore defer further discussion of positron beam experiments to a later article [54].

5. Conclusion

We have presented a comprehensive study of the energy loss and thermalization of positrons in metals. We solved the Boltzmann equation for the positron momentum distribution including both positron–electron and positron–phonon scattering.

The calculated energy loss rates are greater than those presented by Nieminen and Oliva [20] and Perkins and Carbotte [16] by a factor of 2–3 because we take into account the fact that the positrons have an energy distribution of finite width.

Our results conclusively show that, unless the positron trapping rates into vacancy-type defects have much stronger resonances than calculated so far, non-thermal trapping has only a very minor influence on the measurable parameters and cannot lead to major deviations from the conventional trapping model.

Finally, we showed that non-thermal annihilation has a negligible effect on ACAR spectra except at very low temperatures.

Acknowledgments

We are grateful to Malcolm Stott for communications and discussions that initiated this work. KOJ would like to thank the Commission of the European Communities for a Research Grant under the Stimulation Action Scheme, contract no. SCI-0163.

Appendix

In this appendix we examine the long-time behaviour of the positron momentum distribution $g(p, t)$, cf. equation (14), and show that the approach of the mean energy $\bar{E}(t)$ to E_{th} is exponential in this limit. In practice our numerical solutions to the Boltzmann equation (14) show that this limit applies when $\bar{E}$ is below $2E_{th}$.

Our analysis is based on that given in [55] for transport in gases. It is useful to define a deviation function Ψ from

$$g(p, t) = f_{MB}(p)[1 + \Psi(p, t)] \tag{A1}$$

where f_{MB} is the Maxwell–Boltzmann distribution, equation (27). The Boltzmann equation can be written in terms of Ψ as

$$\partial\Psi/\partial t = L\Psi \tag{A2}$$

where L is a linear operator representing the scattering terms. Separating variables t and p and setting $\Psi(p, t) = h(p)a(t)$ one finds that a general solution to equation (A2) can be written

$$\Psi(p, t) = \exp(-\eta_i t)h_i(p) \tag{A3}$$

where $h_i(p)$ is an eigenfunction of L with eigenvalue $-\eta_i$ ($\eta_i \geqslant 0$):

$$Lh_i = -\eta_i h_i. \tag{A4}$$

L is Hermitian [55] because the positron is coupled to a bath of thermal phonons and

electrons. Thus, the functions h_i form a complete orthogonal set and a general solution to equation (A2) can be written:

$$\Psi(p, t) = \sum_i A_i h_i(p) \exp(-\eta_i t) \tag{A5}$$

with the coefficients A_i determined by the initial distribution. Thus, the asymptotic behaviour as $t \rightarrow \infty$ is

$$\Psi(p, t) = A_0 h_0(p) \exp(-\eta_0 t) \qquad t \rightarrow \infty \tag{A6}$$

where η_0 is the smallest eigenvalue of L. From equations (A1), (A6) and (25) it follows that

$$\bar{E} - E_{th} = \text{constant} \times \exp(-t/t_E) \qquad t \rightarrow \infty \tag{A7}$$

where $t_E = 1/\eta_0$, as observed—see section 3.1. The complicated form of L means that it is not possible to find a closed-form expression for t_E since this would involve solving the eigenvalue equation (A4).

References

[1] Sharpe R 1985 *New Scientist* **107** 36
[2] Brandt W and Dupasquier A (ed) 1983 *Positron Solid-State Physics* (Amsterdam: North-Holland)
[3] Hautojärvi P (ed) 1979 *Positrons in Solids* (Berlin: Springer)
[4] Schultz P J and Lynn K G 1988 *Rev. Mod. Phys.* **60** 701
[5] Warburton W K and Shulman M A 1977 *Phys. Lett.* **60A** 448
[6] Gramsch E and Lynn K G 1989 *Phys. Rev.* B **40** 2537
[7] Jackman J A, Hood G M and Schultz R J 1987 *J. Phys. F: Met. Phys.* **17** 1817
[8] Fluss M J, Smedskjaer L C, Chason M K, Legnini D G and Siegel R W 1978 *Phys. Rev.* B **17** 3444
[9] Sharma S C, Berko S and Warburton W K 1976 *Phys. Lett.* **58A** 405
[10] Hehenkamp Th, Kurschat Th and Lühr-Tanck W 1986 *J. Phys. F: Met. Phys.* **16** 981
[11] Lühr-Tanck W, Kurschat Th and Hehenkamp Th 1985 *Phys. Rev.* B **31** 6994
[12] Lühr–Tanck W, Sager A and Ederhof M 1989 *Positron Annihilation* ed L Dorikens-Vanpraet, M Dorikens and D Segers (Singapore: World Scientific) p 512
[13] McMullen T and Stott M J 1986 *Phys. Rev.* B **34** 8935
[14] Puska M J and Manninen M 1987 *J. Phys. F: Met. Phys.* **17** 2235
[15] Carbotte J P and Arora H L 1967 *Can. J. Phys.* **45** 387
[16] Perkins A and Carbotte J P 1970 *Phys. Rev.* B **1** 101
[17] Woll E J and Carbotte J P 1967 *Phys. Rev.* **164** 985
[18] Oliva J 1980 *Phys. Rev.* B **21** 4909
[19] Oliva J 1980 *Phys. Rev.* B **21** 4925
[20] Nieminen R M and Oliva J 1980 *Phys. Rev.* B **22** 2226
[21] Kubica P and Stewart A T 1983 *Can. J. Phys.* **61** 971
[22] Hyodo T, McMullen T and Stewart A T 1986 *Phys. Rev.* B **33** 3050
[23] The correlations between the positron and electron motions, and hence the annihilation rate, are expected to be approximately independent of positron momentum at low momenta. This is because the response time of the electrons, which is of the order of the inverse of the plasma frequency, $\simeq 10^{-16}$ s, is much shorter than the scattering times, of the order of 10^{-14} s, which determine the effective lifetime of the positron quasi-particle states. At higher energies, where plasmon scattering is the dominating scattering mechanims, the two times become comparable. Hence the values of the annihilation rate might be sensitive to positron momentum but the time spent at these high energies is so short that the fraction of positrons annihilating in this period is negligible.
[24] McMullen T 1977 *J. Phys. F: Met. Phys.* **7** 2041
[25] Seeger A 1974 *Appl. Phys.* **4** 1983
[26] Mogensen O E, Eldrup M and Pedersen N J 1985 *Positron Annihilation* ed P C Jain, R M Singru and K P Gopinathan (Singapore: World Scientific) p 756

[27] Nieminen R M, Laakkonen J, Hautojärvi P and Vehanen A 1979 *Phys. Rev.* B **19** 1397
[28] Eldrup M and Jensen K O 1987 *Phys. Status Solidi* a **102** 145
[29] McMullen T 1976 *J. Phys. F: Met. Phys.* **6** L323
[30] Sjölander A and Stott M J 1972 *Phys. Rev.* B **5** 2109
[31] Zhang C, Tzoar N and Platzmann P M 1988 *Phys. Rev.* B **37** 7326
[32] Walker A B, Kong Y and Neilson D 1990 to be published
[33] Weast R C (ed) 1981 *CRC Handbook of Chemistry and Physics* 62nd edn (Baco Raton, FL: CRC Press) p E-45
[34] Ashcroft N W and Mermin N D 1976 *Solid State Physics* (New York: Holt, Rinehart and Winston)
[35] Bergersen B, Pajanne E, Kubica P, Stott M J and Hodges C H 1974 *Solid State Commun.* **15** 1377
[36] Press W H, Flannery B P, Teukolsky S A and Vettering W T 1986 *Numerical Recipes* (Cambridge: Cambridge University Press)
[37] Vassell M O 1970 *J. Math. Phys.* **11** 408
[38] Rees H D 1968 *Phys. Lett.* **26A** 416
[39] Brandt W and Arista N 1979 *Phys. Rev.* A **19** 2317
[40] West R N 1979 *Positrons in Solids* ed P Hautojärvi (Berlin: Springer) p 89
[41] Lynn K G, McKay T and Nielsen B 1987 *Phys. Rev.* B **36** 7107
[42] Hyodo T, McMullen T and Stewart A T 1984 *Can. J. Phys.* **62** 297
[43] Mikeska H-J 1970 *Z. Phys.* **232** 159
[44] Fluss M J, Berko S, Chakraborty B, Lippel P and Siegel R W 1984 *J. Phys. F: Met. Phys.* **14** 2855
[45] Taylor R 1982 *Computer Simulation of Solids* ed C R A Catlow and W C Mackrodt (Berlin: Springer) p 195
[46] Schaefer H-E 1987 *Phys. Status Solidi* a **102** 47
[47] Schaefer H E, Gugelmeier R, Schmolz M and Seeger A 1984 *Microstructural Characterization of Materials by Non-Microscopical Techniques* ed N Hessel Andersen *et al* (Roskilde: Risø National Laboratory) p 489
[48] Schaefer H-E, Stuck W, Banhart F and Bauer W 1987 *Mater. Sci. Forum* **15–18** 117
[49] Hu C-K, Berko S, Gruzalski G R and Warburton W K 1979 *Positron Annihilation* ed R R Hasiguti and K Fujiwara (Sendai: Japanese Institute of Metals) p 231
[50] Walker A B and Jensen K O 1990 *Positron Beams for Solids and Surfaces, Proc. 4th Int. Workshop* ed P Schultz, G Massoumi and P Simpson (New York: American Institute of Physics)
[51] Jensen K O and Walker A B 1990 to be published
[52] Puska M J, Corbel C and Nieminen R M 1990 *Phys. Rev.* B **41** 9980
[53] Nielsen B, Lynn K G and Chen Y-C 1986 *Phys. Rev. Lett.* **57** 1789
[54] Jensen K O and Walker A B 1990 to be published
[55] Smith H and Højgaard Jensen H 1989 *Transport Phenomena* (Oxford: Clarendon) p 10ff